Applied Physics Letters

RESEARCH ARTICLE | MAY 20 2024

Effects of void geometry on two-dimensional monolithic porous phononic crystals

Sharat Paul ; Johannes T. B. Overvelde ; Jacob Hochhalter ; Pai Wang

Appl. Phys. Lett. 124, 212201 (2024)
https://doi.org/10.1063/5.0203024

Applied Physics Letters ARTICLE pubs.aip.org/aip/apl

Effects of void geometry on two-dimensional monolithic porous phononic crystals

Cite as: Appl. Phys. Lett. **124**, 212201 (2024); doi: 10.1063/5.0203024
Submitted: 8 February 2024 · Accepted: 8 May 2024 ·
Published Online: 20 May 2024

Sharat Paul,[1] Johannes T. B. Overvelde,[2] Jacob Hochhalter,[1,a)] and Pai Wang[1,a)]

AFFILIATIONS

[1]Department of Mechanical Engineering, University of Utah, Salt Lake City, Utah 84112, USA
[2]Autonomous Matter Department, AMOLF, Amsterdam 1098 XG, The Netherlands

[a)]**Authors to whom correspondence should be addressed:** jacob.hochhalter@utah.edu and pai.wang@utah.edu

ABSTRACT

Phononic crystals are renowned for their distinctive wave propagation characteristics, notably bandgaps that offer precise control over vibration phenomena, positioning them as a critical material in advanced vibro-elastic engineering and design. We investigate how pore shapes influence the bandgap in continuum two-dimensional phononic crystals made from a single material. Using the square lattice and unit cells with fourfold symmetry, our numerical analyses reveal that the normalized gap size is highly dependent on the minimum ligament width in the structure. Additionally, we find that fine geometric features represented by higher-order Fourier coefficients decrease the gap size. This study offers insight into the design of phononic crystals and vibro-elastic metamaterials for precise wave control through void patterning.

Phononic metamaterials are artificially architected solids with periodic structures, and they are designed to control the propagation of vibro-elastic mechanical waves.[1–3] The bandgap, a frequency range in which waves cannot propagate through the structure, is a crucial property of phononic metamaterials that determines wave manipulation capabilities.[4–6] By engineering bandgaps, we can precisely control the transmission of elastic waves, leading to significant advancements in noise reduction,[7–9] vibration control,[10–13] and seismic wave shielding. Potential applications also include wave guiding[14–17] and filtering,[18–20] vibration damping,[21] acoustic cloaking,[22–24] energy harvesting,[25–29] and medical applications.[30]

Typical phononic crystals with bandgaps may comprise multiple materials with distinct properties, including multi-stubs,[31] multi-materials,[32–34] and local and nonlocal resonators.[35–40] Furthermore, the bandgaps can be extended and shifted by employing multilayered structures.[41] However, the fabrication of such multi-phase and multilayered systems poses considerable complexity. In contrast, monolithic porous periodic structures offer ease of fabrication, even with complex geometries, making them a practical choice for potential industrial applications. With this motivation, our research focuses on bandgaps of monolithic porous phononic crystals, where the material property contrast is between the solid and void phases.

Previous research has demonstrated that introducing pores influences the bandgap properties.[42–46] Here, the shape of voids in a two-dimensional porous phononic metamaterial plays a significant role as it can affect the bandgap properties of the material.[43,47–50] Similarly, the pore shape can also affect and improve other mechanical properties and structural response such as compaction and negative Poisson's ratio.[51–57] An interesting and flexible strategy has been to employ the Fourier series to define the pore shape,[51–53] as a Fourier series can represent any periodic curve. However, the extent to which Fourier series-represented pores can modify the bandgap properties, either enhancing or diminishing them, remains unexplored. Therefore, this study provides a great opportunity to investigate the interplay between pore design and bandgap behavior in metamaterials.

In this study, we investigate the effect of geometric parameters of the pore shape on the bandgap properties of phononic metamaterials in a two-dimensional square array lattice formation. We consider in-plane elastic wave propagation under the plane-strain condition. We use the Fourier series to systematically generate a variety of pore shapes and employ the finite-element method to analyze their bandgap properties. We use the relative gap width as the dimensionless metric to compare the gap size from different void geometries. Our data confirm that a small minimum ligament width in the unit cell geometry is necessary for a large gap size. More intriguingly, our results also show that finer geometry features corresponding to higher-order Fourier coefficients have inverse correlations to the relative gap size.

Based on the mathematical fact that any smooth curve can be well approximated by a Fourier series, we define the pore contour of a diverse set of unit cell designs in the polar coordinates (r, θ) as

$$r(\theta) = r_0\left[1 + \sum_{n=1}^{N} c_n \cos(4n\theta)\right], \tag{1}$$

where $r(\theta)$ is the radial distance from the unit cell center, r_0 denotes the nominal radius, and the factor 4 is included to ensure fourfold symmetry, which is commensurate with the lattice symmetry of a 2D square array. We expect that the individual unit pore shape defined by Eq. (1) will primarily impact wave propagations in the short-wavelength/high-frequency regime, whereas the anisotropy in the long-wavelength/low-frequency regime is mostly dictated by the square lattice arrangement of pores. Here, intricate geometric features can be realized by the Fourier coefficients c_n's, which are dimensionless. In particular, setting all c_n's to zero simplifies the shape to a circle with radius r_0. One crucial design constraint here is to select only the sets of geometric parameters that maintain the structural integrity, i.e., all the solid portions of the periodic structure must be connected. To ensure this, we introduce another pivotal parameter, the minimum ligament width h,[58] defined as

$$h = L - \max_{\theta\in[0,2\pi)} (2r(\theta)\cos(\theta)) > 0, \tag{2}$$

where L is the unit cell size (i.e., the lattice constant of the square array). The constraint of $h > 0$ implies that the solid phase of the phononic crystal cannot have isolated islands. Equations (1) and (2) give us a systematic way to study the effects of pore shape on the bandgap. For a Fourier series up to N terms, there are a total of $N+1$ dimensionless parameters: $c_1, c_2, \ldots, c_N$ and h/L, which collectively specify the void shape completely. We explore this parameter space by varying c_n's and h/L to investigate their combined effects on the bandgap. Our study starts with the geometries shown in Fig. 1(a), where we enforce $h/L = 10\%$ in all cases. Here, we consider $c_1, c_2 \in [-0.3, 0.3]$ with a step size of 0.1 and we set all higher-order $c_n = 0$ for $n \geq 3$. The selected values of c_1 and c_2 results 49 pore shapes shown in Fig. 1(a), where the white areas represent voids. Figure 1(b) illustrates the locations of the minimum ligament length for four example unit cell designs to visualize what h represents. All red line segments in the figure have a length of $h/2$. Additionally, in this study, we also include the cases with nonzero c_n's for n up to 5, investigating the effects of smaller-scale intricacies of the void geometry on bandgaps.

To calculate the dispersion bands, we employ the ABAQUS/STANDARD finite-element platform. Our computational implementation is universally applicable across all geometries. The solid material in every design is characterized by the density of $\rho = 1190\,\text{kg/m}^3$ with transverse and longitudinal wave velocities of $c_T = 1800$ m/s and $c_L = 3100$ m/s,[59] respectively. For every analysis, we construct the finite-element model with a corresponding mesh convergence study. Then, applying Bloch-wave boundary conditions on a single unit cell, we perform eigen-frequency analyses to obtain the dispersion relation. We follow the implementation procedures detailed in a previous study,[42] and example PYTHON-script code files are provided in the supplementary material.

To ensure a fair comparison among all cases, we calculate the relative dimensionless size[42] of the bandgap defined as the ratio of the width to the average frequency of the bandgap,

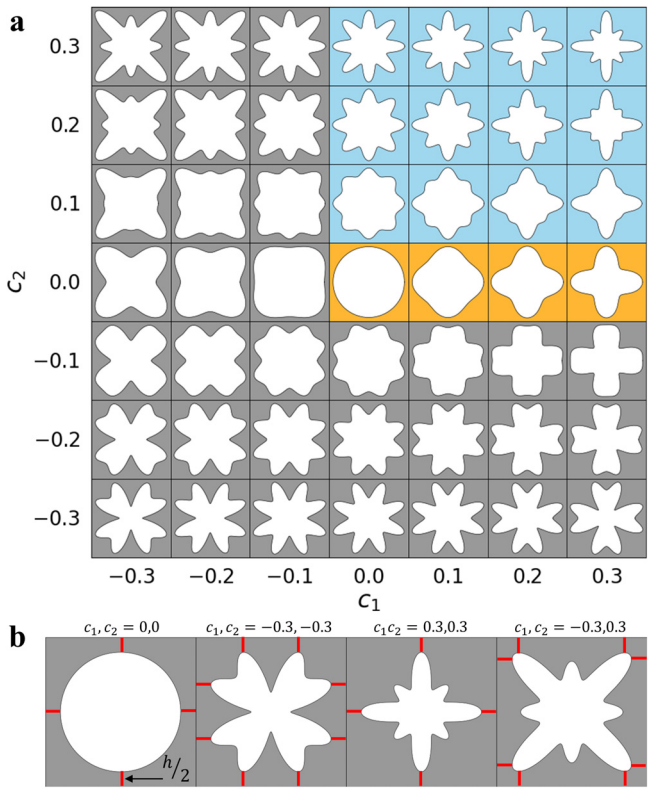

FIG. 1. (a) Example void geometries used in this study. Each shape is generated by Eqs. (1) and (2), with varying Fourier coefficients c_1 and c_2. Some designs are color-coded: yellow for the cases with $(c_1 \geq 0, c_2 = 0)$ and blue for $(c_1 \geq 0, c_2 \geq 0)$. All unit cell designs shown in (a) have $h/L = 10\%$. (b) Example unit cell designs showcasing the locations of minimum-width ligaments. Each red line segment has the length of $h/2$ in its unit cell. Note that, for clear illustration, we use $h/L = 20\%$ for all four examples in (b).

$$\Delta\omega_r = \frac{\omega_{upper} - \omega_{lower}}{(\omega_{upper} + \omega_{lower})/2}, \tag{3}$$

where ω_{upper} and ω_{lower} denote the frequencies of the upper and lower edges of the gap, respectively.

We first compute the dispersion bands over a range of the normalized minimum ligament length h/L, which varies from 5% to 38%. This spans over 18 different h/L values. For each h/L, we generate all 49 unique pore shapes as illustrated in Fig. 1(a). This culminates in a set of 882 geometric configurations. Next, at a fixed value of $h/L = 10\%$, we also study the effects of higher-order Fourier coefficients, c_3, c_4, and c_5 in a total of $4^5 = 1024$ geometries.

We start with the basic unit cell geometry of a perfectly circular void, as depicted in Fig. 2(a). The wave vector components are denoted as (q_x, q_y) in the reciprocal space, and the irreducible Brillouin zone (IBZ)[42] is illustrated by a blue triangle in the reciprocal space, with its center at the Γ point and vertices at the X and M points. To elucidate the existence of phononic bandgaps, we compute the dispersion relations $\omega(\mathbf{q})$ for in-plane mechanical wave propagation. The band structure in Fig. 2(b) manifests as a frequency vs wave vector function for the metamaterial shown in Fig. 2(a). The band structure reveals

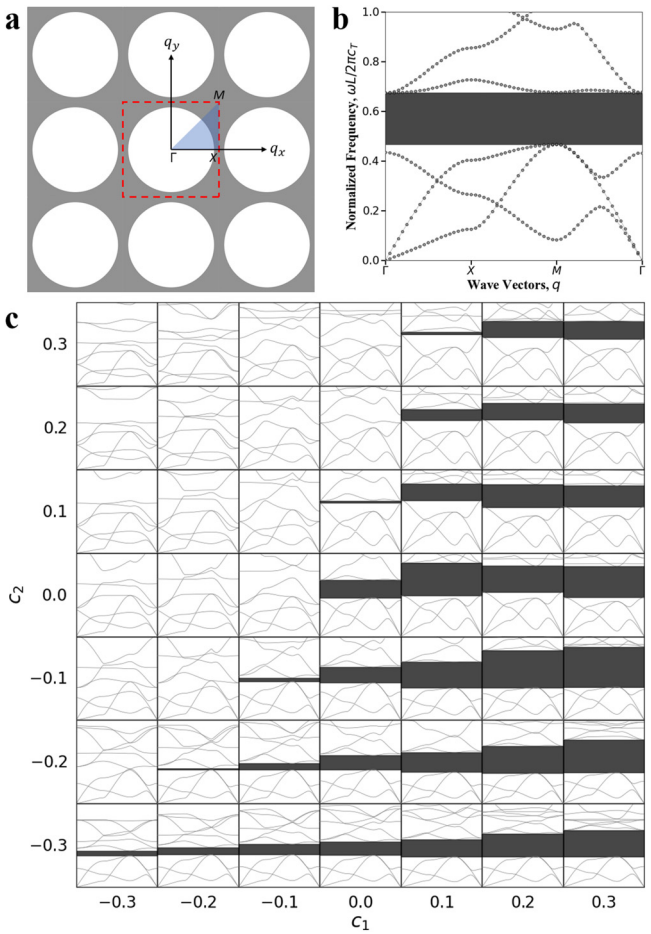

FIG. 2. (a) Illustration of a two-dimensional phononic crystal featuring circular voids with $h/L = 10\%$, showing its unit cell specified by the red dotted boundary. The irreducible Brillouin zone (IBZ) within the reciprocal lattice space is highlighted by the blue triangle ΓXM. (b) Dispersion relations for the phononic crystal in (a). The dark-shaded area indicates the bandgap where dispersion bands (gray curves) are absent. (c) Dispersion relations corresponding to the unit cell configurations illustrated in Fig. 1(a), with the dimensionless minimum ligament width h/L set to 10% in all cases.

regions highlighted in dark gray, where elastic waves of those specific frequencies do not correspond to any wave vector. These spectral ranges, where the elastic waves are forbidden from propagating, constitute the complete phononic bandgaps of the crystal.

Next, we fix h/L at 10% and vary c_1 and c_2. Figure 2(c) presents the band structures corresponding to the pore shapes showcased in Fig. 1(a). The gap above the first three dispersion bands, which is the focus of this study, is highlighted as a dark-shaded rectangle within Figs. 2(b) and 2(c). The gray curves correspond to dispersion relations. All plots in Fig. 2(c) have a maximum normalized frequency $\omega L/2\pi c_T = 1.0$ on the vertical axis, plotted against a set of 60 different wave vectors at the edges of the IBZ. A critical observation from the visualization in Fig. 2(c) is that pore shapes with almost all positive c_1 values consistently present sizable bandgaps. This pattern underscores a significant and robust correlation between c_1 and the bandgap width, indicating the potential of c_1 as a key parameter for maximizing the phononic bandgaps. This also motivates us to quantify the correlations between each geometric parameter and the gap size.

Then, we expand the study to $h/L = 5\%, 6\%, 8\%, \ldots$ up to 38%. We choose to present this specific range because we observe no bandgap can exist for $h/L \geq 38\%$. For each h/L value, we now explore the effect of pore shape while keeping the minimum ligament thickness the same. In Fig. 3, we present the variation of the relative bandgap size, $\Delta\omega_r$ as defined in Eq. (3), as a function of the minimum ligament width for all shape designs from different c_1 and c_2. Each transparent blue data point represents the gap size for a specific void geometry, and each vertical column of data points represents all 49 pore shapes featured in Fig. 1(a) for a fixed h/L. Across all geometries, our findings consistently indicate that an increase in minimum ligament width corresponds to a reduction of the gap size. The overall mean and median of $\Delta\omega_r$ including all cases show bandgap and no-gap are indicated by the solid and dashed black lines, respectively, further illustrating the dominating trend across the entire data set.

We highlight in Fig. 3 some special geometric configurations including the one that exhibits the largest gap. This pore geometry characterized by $c_1 = 0.3$ and $c_2 = -0.1$ emerges as a standout, exhibiting a dominant relative bandgap size of 1.0068 at $h/L = 5\%$ and 0.7526 at $h/L = 10\%$. Figures 4(a) and 4(b) present the detailed band structures corresponding to these configurations. These findings underscore the nuanced yet significant impact that specific geometric modifications can have on the bandgap properties of phononic crystals.

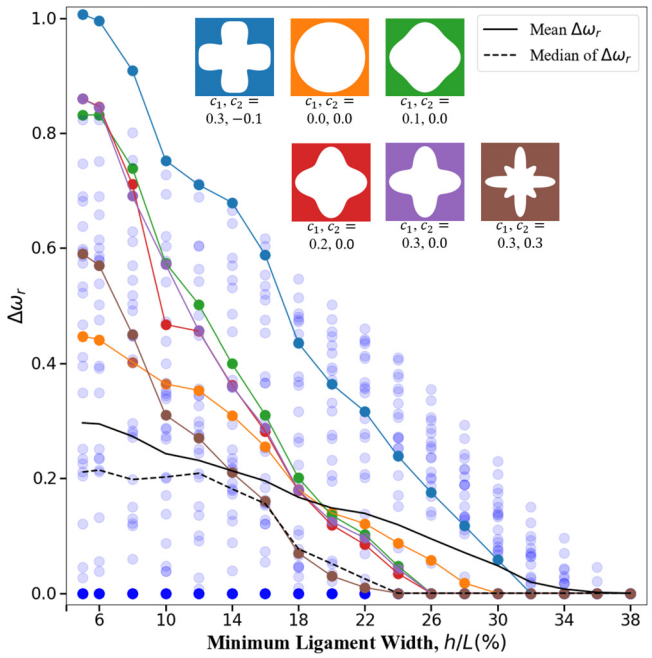

FIG. 3. Relation between the dimensionless gap size ($\Delta\omega_r$) and the dimensionless minimum ligament width (h/L). Each column includes 49 data points corresponding to variations in Fourier coefficients c_1 and c_2 presented in Fig. 1(a). The colorful lines represent the effect of minimum ligament width to the relative bandgap size of some selected shapes including the geometry showing maximum $\Delta\omega_r$.

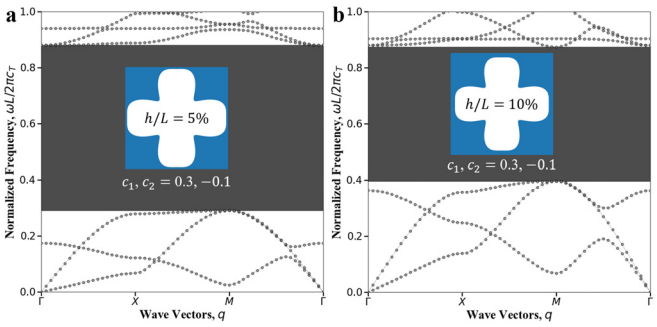

FIG. 4. The band structures of geometry with $c_1 = 0.3$, and $c_2 = -0.1$ with (a) $h/L = 5\%$ and (b) $h/L = 10\%$ while other Fourier coefficients are set to zero.

Using the data presented in Fig. 3, we can also quantify the correlation between the gap size and each of the geometric parameters, including the Fourier coefficients (c_1 and c_2), the nominal pore radius (r_0), the minimum ligament width (h), and the porosity (ϕ), which is defined as the percentage of void space in the unit cell. As shown in Table I, we uncover a strong positive correlation (+0.46) between the relative bandgap width and the c_1 coefficient. This indicates that an increase in c_1 will likely widen the bandgap. In contrast, c_2 shows an inverse correlation of −0.38 with the gap size. Furthermore, contrary to popular belief, the overall porosity ϕ is not strongly correlated with the gap size. Neither is the nominal radius r_0. Importantly, we identify that the minimum ligament width exhibits the most substantial correlation with the bandgap width, with a pronounced negative coefficient of −0.48. This illustrates that as we decrease h, the relative bandgap size increases, which provides a basic strategy for designs to achieve desirable bandgap sizes. Through this correlative analysis, we comprehensively understand how each geometric parameter influences the gap size. Such insights empower us to tailor the design precisely, optimizing for either targeted bandgap width in various application scenarios.

In addition, we also investigate the effects of higher-order Fourier coefficients, namely c_3, c_4, and c_5 in Eq. (1). As previous findings show that a gap exists in almost all pore shapes within positive ranges of the Fourier coefficients $c_1, c_2 \geq 0$, we now narrow our focus to the significant subset of design generated by all positive Fourier coefficients. We examine the evolution of pore shapes by varying each of these coefficients from 0 to 0.3 in increments of 0.1. In Fig. 5(a), we show how the pores change due to the inclusion of $c_3 \geq 0$ and $c_4 \geq 0$ while fixing $c_1 = c_2 = 0$ and $h/L = 10\%$. This visualization makes it apparent that nonzero higher-order coefficients introduce geometric features at smaller length scales.

TABLE I. Correlation coefficients between each of the geometric parameters with the relative bandgap size ($\Delta\omega_r$). The coefficients can range from 1, indicating a perfect positive correlation, to −1, signifying a perfect negative correlation. Note that, although five geometric parameters are listed below, we only have three independent ones (c_1, c_2, and h/L are used in this study).

Geometric parameter	Correlation coefficient
c_1	+0.46
c_2	−0.38
h/L	−0.48
ϕ	+0.17
r_0/L	+0.20

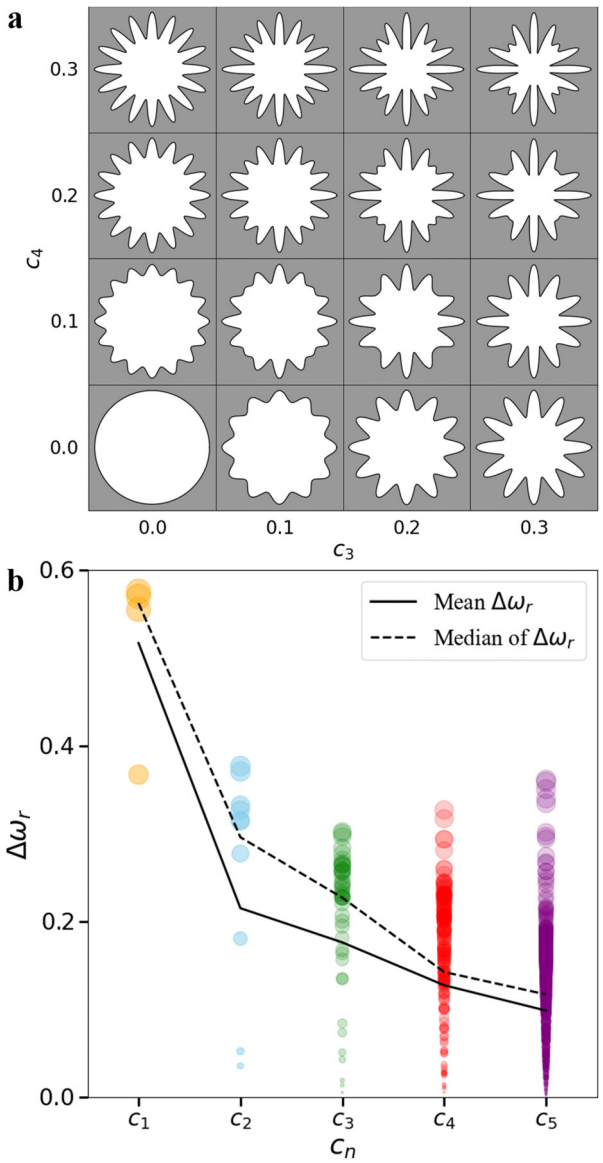

FIG. 5. (a) Influence of higher-order Fourier coefficients, $c_3 \geq 0$ and $c_4 \geq 0$, on pore shapes. We have $c_1 = c_2 = c_5 = 0$ and $h/L = 10\%$ for all shapes shown here. (b) Relative gap size ($\Delta\omega_r$) from pore shapes specified by non-negative Fourier coefficients c_1 through c_5. Each circle represents one particular design, while each column represents gap sizes corresponding to varying all lower-order coefficients. For example, the c_1 column has four yellow points corresponding to the four yellow-colored shapes in Fig. 1(a), and the c_2 column has 12 blue points corresponding to the twelve blue-colored shapes in Fig. 1(a). Likewise, the c_3 column includes shapes with varying c_1, c_2, and nonzero c_3 while keeping $c_4 = c_5 = 0$. In total, there are $4^5 = 1024$ data points in this plot.

We then calculate the relative bandgap size for all new geometries prescribed by non-negative higher-order Fourier coefficients c_n up to $n = 5$. In Fig. 5(b), we present the results of our extensive parameter sweep. The data show that higher-order Fourier coefficients do not help increase the gap size at all. Moreover, the mean and median gap sizes indicate a clear decreasing trend for including the higher-order coefficients. Therefore, we find that geometric features at smaller length scales tend to reduce the gap sizes, even when the minimum ligament width h is held constant. Figure 5(b) reveals that when considering Fourier descriptors up to c_5, the optimal geometry for maximizing the relative bandgap size within the positive domain of c_n solely depends on c_1. Specifically, the shape that presents the largest relative bandgap has $c_1 = 0.1$ and $c_n = 0$ for $n > 1$. This finding underscores the predominant influence of the first Fourier descriptor on the relative bandgap size.

To quantify this negative effect of higher-order Fourier terms on the gap size, we calculate correlation coefficients between each c_n and $\Delta\omega_r$ based on the data in Fig. 5(b). Table II demonstrates the individual significance of c_n's for bandgap engineering. The coefficient c_1 still shows a robust positive correlation of +0.66 in this new set of data, reinforcing its critical role—a larger c_1 is indicative of a wider bandgap. In contrast, the influence of c_2 and c_3 appears to be marginal, with correlation coefficients close to zero at +0.03 and −0.05, respectively. However, as we proceed to higher-order terms, a consistent pattern emerges: Each subsequent coefficient exhibits a stronger negative correlation with the relative bandgap size, culminating in c_5 with a correlation coefficient of −0.32. The progression from c_1 to c_5 reveals a fact that can serve as a useful design strategy: While c_1 alone can significantly widen the bandgap, the incorporation of higher-order coefficients with positive values will result in narrower gaps.

Table II delineates the substantial impact of the Fourier descriptors c_1 and c_5 on the size of the bandgap. This is based on the non-negative range of higher-order Fourier coefficients c_3, c_4, and c_5, and it shows a strong inverse correlation with the relative bandgap size. Motivated by this insight, we conduct further analysis in the negative range of c_5 on three pore geometries specified by $c_1 = 0.3$, $c_5 = -0.1, -0.2, -0.3$, and keeping other c_n at zero. These configurations achieve a relative bandgap size of $\Delta\omega_r = 0.6713, 0.6749$, and 0.6062, respectively, surpassing all 1024 shapes examined in Fig. 5(b). These results further reinforce the correlation between the Fourier coefficients and the relative bandgap size, as identified in Table II.

In this data-driven study, we establish the significance of the unit cell minimum ligament width, h, which shows a very strong negative correlation with the bandgap size of porous phononic crystals. Our findings reinforce the argument that smaller ligament widths lead to wider bandgaps. This is a useful insight for precise wave control applications, offering advancements in areas like acoustic filtering and vibration isolation. Furthermore, the bandgap becomes narrower when the design includes fine geometric features at small length scales represented by higher-order Fourier coefficients. This finding is useful for design strategies in many scenarios and can be used as a guideline for not only 2D but also 3D continuum porous phononic crystals.

TABLE II. Correlation between Fourier coefficients (c_n) and the relative bandgap size ($\Delta\omega_r$) with a fixed $h/L = 10\%$.

Fourier coefficients	Correlation coefficient
c_1	+0.66
c_2	+0.03
c_3	−0.05
c_4	−0.18
c_5	−0.32

See the supplementary material for detailed source codes used for the numerical analyses and a comprehensive README file for guidance on executing the codes. We have also provided the raw data set corresponding to the results presented in Fig. 2(b). Furthermore, we briefly describe how Eq. (1) might influence the symmetry of the unit cell, along with the statistical analysis of the bandgap data presented.

We acknowledge the support from P.W.'s start-up research funds of the Department of Mechanical Engineering at the University of Utah. This work is part of the Dutch Research Council (NWO) and was in part performed at the research institute AMOLF. The support and resources from the Center for High Performance Computing at the University of Utah are gratefully acknowledged. The authors are grateful to Hongsup Oh, Ryan Alberdi, and Joshua Robbins for inspirational discussions.

AUTHOR DECLARATIONS

Conflict of Interest

The authors have no conflicts to disclose.

Author Contributions

Sharat Paul: Conceptualization (lead); Data curation (lead); Formal analysis (lead); Investigation (lead); Methodology (lead); Software (lead); Validation (lead); Visualization (lead); Writing – original draft (lead); Writing – review & editing (lead). **Johannes T.B. Overvelde:** Conceptualization (supporting); Funding acquisition (equal); Methodology (supporting); Project administration (equal); Resources (supporting); Software (supporting); Writing – review & editing (supporting). **Jacob Hochhalter:** Conceptualization (equal); Funding acquisition (equal); Project administration (equal); Resources (equal); Supervision (equal); Writing – review & editing (equal). **Pai Wang:** Conceptualization (equal); Formal analysis (equal); Funding acquisition (equal); Investigation (equal); Methodology (equal); Project administration (equal); Resources (equal); Software (equal); Supervision (equal); Validation (equal); Visualization (equal); Writing – original draft (equal); Writing – review & editing (equal).

DATA AVAILABILITY

The data that support the findings of this study are available from the corresponding authors upon reasonable request.

REFERENCES

[1]M. Sigalas and E. N. Economou, "Band structure of elastic waves in two dimensional systems," Solid State Commun. **86**, 141–143 (1993).
[2]M. S. Kushwaha, P. Halevi, L. Dobrzynski, and B. Djafari-Rouhani, "Acoustic band structure of periodic elastic composites," Phys. Rev. Lett. **71**, 2022–2025 (1993).

[3]M. S. Kushwaha, P. Halevi, G. Martínez, L. Dobrzynski, and B. Djafari-Rouhani, "Theory of acoustic band structure of periodic elastic composites," Phys. Rev. B **49**, 2313–2322 (1994).
[4]O. R. Bilal and M. I. Hussein, "Ultrawide phononic band gap for combined in-plane and out-of-plane waves," Phys. Rev. E **84**, 065701 (2011).
[5]T. Liu, F. Chen, S. Liang, H. Gao, and J. Zhu, "Subwavelength sound focusing and imaging via gradient metasurface-enabled spoof surface acoustic wave modulation," Phys. Rev. Appl. **11**, 034061 (2019).
[6]M. I. Rosa, R. K. Pal, J. R. Arruda, and M. Ruzzene, "Edge states and topological pumping in spatially modulated elastic lattices," Phys. Rev. Lett. **123**, 034301 (2019).
[7]J. Chen, Y. Zhang, Y. Yu, Y. Zhai, H. Nguyen, S. Tracy, X. Zhou, and G. Huang, "Broadband acoustic attenuation in microperforated meta-shells with ventilation," Appl. Phys. Lett. **122**, 231701 (2023).
[8]C. Lagarrigue, J.-P. Groby, O. Dazel, and V. Tournat, "Design of metaporous supercells by genetic algorithm for absorption optimization on a wide frequency band," Appl. Acoust. **102**, 49–54 (2016).
[9]V. Romero-García, G. Theocharis, O. Richoux, A. Merkel, V. Tournat, and V. Pagneux, "Perfect and broadband acoustic absorption by critically coupled sub-wavelength resonators," Sci. Rep. **6**, 19519 (2016).
[10]M. D. Guild, A. J. Hicks, M. R. Haberman, A. Alù, and P. S. Wilson, "Acoustic scattering cancellation of irregular objects surrounded by spherical layers in the resonant regime," J. Appl. Phys. **118**, 164903 (2015).
[11]C. Chen, Z. Du, G. Hu, and J. Yang, "A low-frequency sound absorbing material with subwavelength thickness," Appl. Phys. Lett. **110**, 221903 (2017).
[12]S. Sergeev, R. Fleury, and H. Lissek, "Ultrabroadband sound control with deep-subwavelength plasmacoustic metalayers," Nat. Commun. **14**, 2874 (2023).
[13]Y. Chen, B. Zhao, X. Liu, and G. Hu, "Highly anisotropic hexagonal lattice material for low frequency water sound insulation," Extreme Mech. Lett. **40**, 100916 (2020).
[14]M. Kafesaki, M. M. Sigalas, and N. García, "Frequency modulation in the transmittivity of wave guides in elastic-wave band-gap materials," Phys. Rev. Lett. **85**, 4044–4047 (2000).
[15]E. Muzar and J. A. Stotz, "Defect-free phononic crystal waveguides on GaAs," Crystals **13**, 1540 (2023).
[16]A. A. Oliner, "Waveguides for acoustic surface waves: A review," Proc. IEEE **64**(5), 615–627 (1976).
[17]M. Roshdy, T. Chen, S. Nakhmanson, and O. R. Bilal, "Tunable ferroelectric auxetic metamaterials for guiding elastic waves in three-dimensions," Extreme Mech. Lett. **59**, 101966 (2023).
[18]M. Sigalas, "Defect states of acoustic waves in a two-dimensional lattice of solid cylinders," J. Appl. Phys. **84**, 3026–3030 (1998).
[19]G. Ma, M. Yang, Z. Yang, and P. Sheng, "Low-frequency narrow-band acoustic filter with large orifice," Appl. Phys. Lett. **103**, 011903 (2013).
[20]N. Boechler, C. Daraio, R. K. Narisetti, M. Ruzzene, and M. Leamy, *Analytical and Experimental Analysis of Bandgaps in Nonlinear One Dimensional Periodic Structures* (Springer, 2010), pp. 209–219.
[21]M. I. Hussein and M. J. Frazier, "Band structure of phononic crystals with general damping," J. Appl. Phys. **108**, 093506 (2010).
[22]S. A. Cummer, B.-I. Popa, D. Schurig, D. R. Smith, J. Pendry, M. Rahm, and A. Starr, "Scattering theory derivation of a 3D acoustic cloaking shell," Phys. Rev. Lett. **100**, 024301 (2008).
[23]X. Zhu, B. Liang, W. Kan, X. Zou, and J. Cheng, "Acoustic cloaking by a superlens with single-negative materials," Phys. Rev. Lett. **106**, 014301 (2011).
[24]X. Xu, C. Wang, W. Shou, Z. Du, Y. Chen, B. Li, W. Matusik, N. Hussein, and G. Huang, "Physical realization of elastic cloaking with a polar material," Phys. Rev. Lett. **124**, 114301 (2020).
[25]Y. Li, E. Baker, T. Reissman, C. Sun, and W. K. Liu, "Design of mechanical metamaterials for simultaneous vibration isolation and energy harvesting," Appl. Phys. Lett. **111**, 251903 (2017).
[26]G. Lee, D. Lee, J. Park, Y. Jang, M. Kim, and J. Rho, "Piezoelectric energy harvesting using mechanical metamaterials and phononic crystals," Commun. Phys. **5**, 94 (2022).
[27]A. Ikei, J. Wissman, K. Sampath, G. Yesner, and S. N. Qadri, "Tunable in situ 3D-printed PVDF-TrFE piezoelectric arrays," Sensors **21**, 5032 (2021).
[28]Z. Lin, H. Al Ba'ba'a, and S. Tol, "Piezoelectric metastructures for simultaneous broadband energy harvesting and vibration suppression of traveling waves," Smart Mater. Struct. **30**, 075037 (2021).
[29]M. N. Hasan, T. E. Greenwood, R. G. Parker, Y. L. Kong, and P. Wang, "Fractal patterns in the parameter space of a bistable duffing oscillator," Phys. Rev. E **108**, L022201 (2023).
[30]B. Peng, H. Xu, F. Song, P. Wen, Y. Tian, and Y. Zheng, "Additive manufacturing of porous magnesium alloys for biodegradable orthopedic implants: Process, design, and modification," J. Mater. Sci. Technol. **182**, 79 (2024).
[31]P. Jiang, X.-P. Wang, T.-N. Chen, and J. Zhu, "Band gap and defect state engineering in a multi-stub phononic crystal plate," J. Appl. Phys. **117**, 154301 (2015).
[32]S. G. Konarski and C. J. Naify, "Elastic bandgap widening and switching via spatially varying materials and buckling instabilities," JASA Express Lett. **1**, 015602 (2021).
[33]Y. Li, Y. Luo, and X. Zhang, "Topological design of phononic crystals for multiple wide band gaps," J. Sound Vib. **529**, 116962 (2022).
[34]Y. Lu, Y. Yang, J. K. Guest, and A. Srivastava, "3-D phononic crystals with ultra-wide band gaps," Sci. Rep. **7**, 43407 (2017).
[35]P. Celli, B. Yousefzadeh, C. Daraio, and S. Gonella, "Bandgap widening by disorder in rainbow metamaterials," Appl. Phys. Lett. **114**, 091903 (2019).
[36]L. Raghavan and A. S. Phani, "Local resonance bandgaps in periodic media: Theory and experiment," J. Acoust. Soc. Am. **134**, 1950–1959 (2013).
[37]K. H. Matlack, A. Bauhofer, S. Krödel, A. Palermo, and C. Daraio, "Composite 3D-printed metastructures for low-frequency and broadband vibration absorption," Proc. Natl. Acad. Sci. U. S. A. **113**, 8386–8390 (2016).
[38]A. Bossart and R. Fleury, "Extreme spatial dispersion in nonlocally resonant elastic metamaterials," Phys. Rev. Lett. **130**, 207201 (2023).
[39]A. A. Bossart, "Nonlocally-resonant metamaterials," Doctoral thesis (EPFL, 2023).
[40]D. Torrent, Y. Pennec, and B. Djafari-Rouhani, "Resonant and nonlocal properties of phononic metasolids," Phys. Rev. B **92**, 174110 (2015).
[41]X. Zhou, Y. Xu, Y. Liu, L. Lv, F. Peng, and L. Wang, "Extending and lowering band gaps by multilayered locally resonant phononic crystals," Appl. Acoust. **133**, 97–106 (2018).
[42]P. Wang, J. Shim, and K. Bertoldi, "Effects of geometric and material nonlinearities on tunable band gaps and low-frequency directionality of phononic crystals," Phys. Rev. B **88**, 014304 (2013).
[43]Y. Liu, J. Y. Su, and L. Gao, "The influence of the micro-topology on the phononic band gaps in 2D porous phononic crystals," Phys. Lett. A **372**, 6784–6789 (2008).
[44]X.-X. Su, Y.-F. Wang, and Y.-S. Wang, "Effects of Poisson's ratio on the band gaps and defect states in two-dimensional vacuum/solid porous phononic crystals," Ultrasonics **52**, 255–265 (2012).
[45]K. Wang, Y. Liu, T. Liang, and B. Wang, "Band structures in fractal grading porous phononic crystals," J. Phys. Chem. Solids **116**, 367–374 (2018).
[46]Y. Liu, X.-Z. Sun, and S.-T. Chen, "Band gap structures in two-dimensional super porous phononic crystals," Ultrasonics **53**, 518–524 (2013).
[47]S. C. Paul, H. Oh, J. Hochhalter, and P. Wang, "Effects of pore shape contour on band gaps of 2D periodic structures," in Bulletin of the American Physical Society (2023).
[48]F. Javid, P. Wang, A. Shanian, and K. Bertoldi, "Architected materials with ultra-low porosity for vibration control," Adv. Mater. **28**, 5943–5948 (2016).
[49]Z.-G. Chen and Y. Wu, "Tunable topological phononic crystals," Phys. Rev. Appl. **5**, 054021 (2016).
[50]M. Lyu, G. Xu, B. Cheng, and Z. Xia, "Parametric analysis: Compressibility of rubber on bandgap for phononic crystals," Mod. Phys. Lett. B **38**, 2450168 (2023).
[51]J. T. B. Overvelde, S. Shan, and K. Bertoldi, "Compaction through buckling in 2D periodic, soft and porous structures: Effect of pore shape," Adv. Mater. **24**, 2337–2342 (2012).
[52]M. Lyu, F. Zhang, B. Cheng, L. Dai, and Z. Xia, "Study on influence of parameters of buckling behavior in soft mechanical metamaterials," Mod. Phys. Lett. B **38**, 2450118 (2024).
[53]K. A. Khan, M. H. Alshaer, and M. A. Khan, "A novel twofold symmetry architected metamaterials with high compressibility and negative Poisson's ratio," Adv. Eng. Mater. **23**, 2001041 (2021).

[54]M. S. Elsayed and D. Pasini, "Analysis of the elastostatic specific stiffness of 2D stretching-dominated lattice materials," Mech. Mater. **42**, 709–725 (2010).
[55]Y. Chen, T. Li, F. Scarpa, and L. Wang, "Lattice metamaterials with mechanically tunable Poisson's ratio for vibration control," Phys. Rev. Appl. **7**, 024012 (2017).
[56]K. K. Dudek, J. A. Iglesias Martínez, G. Ulliac, L. Hirsinger, L. Wang, V. Laude, and M. Kadic, "Micro-scale mechanical metamaterial with a controllable transition in the Poisson's ratio and band gap formation," Adv. Mater. **35**, 2210993 (2023).
[57]J. T. Overvelde and K. Bertoldi, "Relating pore shape to the non-linear response of periodic elastomeric structures," J. Mech. Phys. Solids **64**, 351–366 (2014).
[58]J. Shim, P. Wang, and K. Bertoldi, "Harnessing instability-induced pattern transformation to design tunable phononic crystals," Int. J. Solids Struct. **58**, 52–61 (2015).
[59]M. Maldovan and E. L. Thomas, *Periodic Materials and Interference Lithography: For Photonics, Phononics and Mechanics* (John Wiley & Sons, 2009).